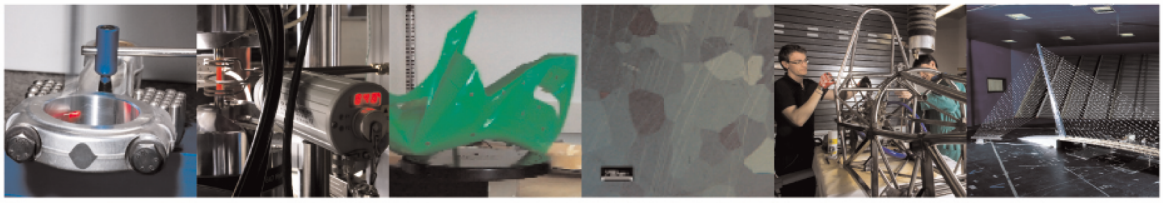

# Comparison of the reduction behavior through blast furnace sludge of two industrial jarosites

Mombelli D.;Dall'Osto G.;Trombetta V.;Mapelli C.



# Comparison of the reduction behavior through blast furnace sludge of two industrial jarosites

D. Mombelli[1,*], G. Dall'Osto[1], V. Trombetta[1], C. Mapelli[1]
[1]Dipartimento di Meccanica, Politecnico di Milano, Via La Masa 1, 20156 Milano, Italy
*corresponding author: davide.mombelli@polimi.it

## Abstract

Jarosite is the main by-product of the zinc hydrometallurgical Roast-Leach-Electrowin (RLE) process and contains 35-50 wt.% of iron oxide which can be recovered for low-grade iron production. As a follow-up of the positive experience of an industrial jarosite reduction by using blast furnace sludges, this paper proposes the same procedure applied to another industrial jarosite different in S, Pb, Ca and Zn concentration, with the aim of investigating the effect of the origin of the jarosite on the best BFS/jarosite ratio to be implemented in the production of self-reducing briquettes.

Thermogravimetric coupled with differential scanning calorimetry analysis has been conducted in argon atmosphere on three BFS/jarosite/quartz mixes to replicate the same C/$Fe_2O_3$ ratio (0.131, 0.261, 0.523) and basicity (0.504) used in the previous investigation. Coherently with the results obtained with the first jarosite (J1), also for the new jarosite (J2), the highest iron oxide reduction was obtained for a C/$Fe_2O_3$ ratio of 0.261. Consequently, the reducibility of jarosite plus blast furnace sludge is not affected by the chemical composition of the starting jarosite from the point of view of the overall iron reduction yield.

## Keywords

Jarosite; blast furnace sludges; carbothermal reduction; TG-DSC; waste management; circular economy

## 1 Introduction

Jarosite is the main by-product of the zinc hydrometallurgical Roast-Leach-Electrowin (RLE) process [1]. The main steps of this process are the roasting of zinc sulfide, its leaching in sulfuric acid, the purification of the resulting zinc sulfate solution and the recovery of high purity metallic zinc by electrowinning [2]. Although most of the zinc is converted during roasting, a significant percentage reacts with iron impurities to form zinc ferrite ($ZnFe_2O_4$). This iron compound must be eliminated from the solution to prevent its persistent accumulation. Over the years, the zinc industry has developed a number of technologies to precipitate the dissolved iron in a readily filterable form [3,4]. One of them, known as Jarosite Process, was developed as an important solution purification technique for the removal of iron at 90-100 °C in the zinc industries [5].

Because of the great significance of jarosite in both mineralogy and hydrometallurgy, the synthesis and precipitation of the different members of the jarosite family have been extensively studied over the past 50 years, as the factors affecting their precipitation (e.g., solution pH, temperature, maintenance time) [6–8]. In addition to more traditional process parameters, the role of impurities (e.g., As, Ga, Cd, Sc and phosphates) in the jarosite precipitation has also been studied in depth [9–16]. At equilibrium, the formation of mineral jarosite is expressed by Reaction 1, where X represents $H_3O^+$, $Na^+$, $K^+$, $NH_4^+$, $Ag^+$ or $0.5Pb^{2+}$ [17,18].

$$3Fe_2(SO_4)_3 + X_2SO_4 + 12H_2O \leftrightarrow 2XFe_3(SO_4)_2(OH)_6 + 6H_2SO_4 \quad (1)$$

Furthermore, synthetic jarosite compounds, without a mineral counterpart, have been experimentally investigated, with both positive and negative results, at laboratory scale by exploiting specific cations such as $Ce^+$, $Li^+$, $½Pb^{2+}$ ,$Rb^+$ and $Tl^+$ [19–21].

Industrial jarosite wastes are considered hazardous due to the presence and mobility of toxic metals contained inside them, as far as their acidic pH [22]. Therefore, stabilization treatments, such as the Jarofix®, are required to limit the leaching of toxic metals (e.g., Cd, Cu, Pb, Zn and Hg) and soluble salts as chlorides [3,23,24]. Another possibility to avoid the environmental problems caused by the disposal and uncontrolled leaching is the developing of cleaner processes for the jarosite reutilization [25,26]. Deqing Zhu et al. developed a new pyrometallurgical route for the separation and recovery of Fe, Zn, In, Ga and S from hazardous jarosite residues based on thermal decomposition and desulfurization of jarosite, and its exploitation for the separation and recovery of metallic elements [27]. Rama et al. investigated the recovery of jarosite leach residues by a two-step pyrometallurgical process. More specifically, the wastes were firstly melted in an oxidizing atmosphere followed by the reduction of the liquid metal to produce a disposable clean slag and the recovery of the metals contained in the starting residue (e.g., Zn, Pb, Cu and Ag) [28]. Vinals, Roca and Patiño proposed several hydrometallurgical solutions for the recovery of precious elements (i.e., Au and Ag) by alkaline decomposition and cyanidation of different jarosites [29–33]. Mombelli et al. utilized coke as reducing agent to recover the residual iron content within jarosite sludges through an Arc Transferred Plasma (ATP) reactor and characterized both the slag and cast iron from a metallurgical and environmental point of view. The aim of the work was the production of a valuable Fe-based product and an inert unreducible slag [34]. However, due to coke production cost and huge environmental impact (~6.7% of global $CO_2$ emissions) alternative reductants are required for the competitiveness of the process [35]. As a result, the exploitation of the residual fraction of unburned coke of blast furnace sludges (BFS) and their use as reducing agents has been widely demonstrated in recent years [36–39].

Blast furnace sludges are one of the main by-products coming from the purification of the blast furnace top gases. These gases exit at a temperature of 200-300 °C and contain a high quantity of powders from the bed of fusion (about 20 kg of powders per ton of pig iron) [40]. Due to the high C and Fe content of the sludges, it can be considered worthwhile to recycle them by charging-back to the blast furnace. The recovery of the unburnt coke inside the BFS would also be advantageous from both the environmental and economic point of view, as it would no longer be considered as an output, but, on the contrary, as an input material. Consequently, the process would require a lower amount of coke, thus decreasing the emissions and carbon tax of the process [41]. However, the direct recycling of flue dusts is not suggested since the presence of undesirable elements (e.g., Zn, Pb and alkali metals) that can cause operational issues. Furthermore, the fine-grained character of the BFS prevents them to serve as a feeding material [41–43].

Although the use of BFS as reducing agent has been already confirmed [36], no precise study has been conducted to investigate the influence of the chemical composition of the starting jarosite from the point of view of metal production. Therefore, this paper proposes the utilization of blast furnace sludges as reductant for a new industrial jarosite sample, with the aim to define the best BFS/jarosite ratio for the production and subsequent utilization of self-reducing briquettes. Such knowledge would not only allow to understand whether the best $C/Fe_2O_3$ ratio depends on the chemistry of the jarosite, but also whether specific pretreatments (either hydrometallurgical or pyrometallurgical) have to be carried out on the jarosite to obtain the highest iron production yield. Consequently, this study should be understood as an expansion of the previous work and a step further in the low emission iron production by industrial waste materials.

## 2 Materials and methods

### 2.1 Jarosite and Blast Furnace Sludge Characterization

The new industrial jarosite (jarosite 2 – J2) used in this work was thermally and chemically compared with a previously characterized jarosite sample (jarosite 1 – J1) [36].

Jarosite 2 was supplied in a form of a yellow-greenish sludge. Once received, the as-supplied jarosite was dried at 105 °C for 24 h to remove the excess of water and roasted at 1000 °C for 1 h in a muffle furnace to oxidize most of sulfur present. Dried and roasted samples was chemically and mineralogically investigated through Energy Dispersive (ED-XRF) and Wavelength Dispersive X-ray Fluorescence (WD-RXF), X-Ray Diffraction analysis (XRD) and Scanning Electron Microscopy with Energy Dispersive X-Ray Spectrometry (SEM-EDS). ED-XRF was carried out by means of Ametec Spectro Xepos spectrometer (Ametek Inc, Berwyn, Pennsylvania, USA) while WD-XRF was carried out by means of a Bruker S8 Tiger (Bruker Corporation, Billerica, Massachusetts, USA) according to EN 15309:2007 standard. XRD was performed by means of a Rigaku SmartLab SE diffractometer (Rigaku Corporation, Tokyo, Japan) in θ-θ configuration. Incident X-ray beam was produced by exciting a Cu tube (Kα, λ = 1.54 Å) at 40 kV, 40 mA. Diffracted beam was detected from 5 to 90 °2θ through a 1D D/teX Ultra 250 detector featured by XRF suppression filter. The powdered material was scanned at 1 °/min with a step size of 0.02 ° and rotated at 30 rpm. SEM analysis was carried out by mean of a Zeiss Sigma 300 Field Emission Gun SEM (FEG-SEM) (Carl Zeiss AG, Oberkochen, Germany) equipped with an Oxford Xmax Ultim 65 Energy-Dispersive X-Ray Spectroscopy (EDS) probe (Oxford INCA, Oxford Instruments, High Wycombe, UK). The blast furnace sludge used in the mixture is the same used by Mombelli et. al. in previous works [36,38,39,44] and was subjected to the drying process only.

### 2.2 Thermal reduction investigation

The thermal reduction behavior of the J2-jarosite was investigated by means of Thermo-Gravimetric Differential Scanning Calorimetry (TG-DSC) heating 20 mg of sample up to 1200 °C (rate: 30 °C/min) under Ar flow (2 Nl/h) in a Setaram Labsys simultaneous thermal analysis machine (Setaram Solutions, Caluire, France). Three mixtures, with growing BFS/jarosite ratio have been prepared. The inert atmosphere was used to prevent the carbon combustion and thus investigate the best C/$Fe_2O_3$ ratio for the iron oxide reduction, as the mixture mass loss would linearly increase in the case of air atmosphere [36]. High purity quartz (>95% $SiO_2$) was added to correct the starting binary basicity index (BI) of each mixture and obtain the same CaO/$SiO_2$ ratio (0.504) used in the previous work of Mombelli et al. to maintain a continuity and allow direct comparison with previous results [36]. The mixtures labelling and material percentages are summarized in Table 1.

Table 1. Labelling and characteristics of BFS plus J2-jarosite mixtures.

| ID | BFS respect to Jarosite (%) | Quartz respect to Jarosite (%) | C/$Fe_2O_3$ | BI |
|---|---|---|---|---|
| **A** | 16.51 | 16.54 | 0.131 | 0.504 |
| **B** | 35.93 | 16.35 | 0.261 | 0.504 |
| **C** | 89.10 | 15.82 | 0.523 | 0.504 |

The reduction behavior of the J2-jarosite plus BFS mixtures (J2-BFS) were compared to a theoretical thermodynamic model for mass loss assessment, which was previously used by Mombelli et al. to study the reduction behavior of J1-jarosite plus BFS mixtures (J1-BFS) [36,39]. The model assumes the direct reduction of the reducible oxides exclusively by the carbon introduced in the mixture, using the starting chemical composition of the mix as input

data. The output values regard the percentages of metal and slag formed, the C and FeO residues, and the actual mass loss, which is computed as the sum of three different contributes:

- loss of the oxygen contained in non-ferrous reducible oxides at 1200 °C;
- loss of the oxygen contained in the $Fe_2O_3$ content when it is reduced to Fe by taking into account the step partial reduction ($Fe_2O_3$ → $Fe_3O_4$ → FeO → Fe);
- loss of all the carbon needed to reduce all the reducible oxides [36,39].

## 3 Results and discussion

### 3.1 Raw materials characterization

The chemical composition of jarosite feedstocks is reported in Table 2 as well as SEM-EDS characterization of J2-jarosite (Figure 1, Table 3).

After the oven drying treatment, the as-supplied J2-jarosite sludges lost roughly 43% of its initial mass due to the evaporation of the excess of water. This amount is largely higher than the corresponding evaporation observed during the J1-jarosite drying (~30%) [34]. As highlighted by the XRD spectrum (Figure 2b), the dried J2-jarosite is composed by natrojarosite, plumbojarosite, bassanite, quartz and sulfur. These compounds are similar to those previously identified in the J1-jarosite, except for the absence of a significant fraction of franklinite (Figure 2a) [34]. This is not surprising, since the final composition of jarosite sludges depends on the neutralizing agents used during the hydrolysis step and the subsequent neutralization of thickened jarosite solids [45]. During the following roasting stage, an additional mass loss of 50% was observed for the J2-jarosite. This is mainly associated to jarosite decomposition with a subsequent increase of the iron oxide amount and release of $SO_3$ due to free sulfur oxidation. This value is almost twice than the mass loss registered during J1-jarosite roasting (~26-29%) [34]. This means that starting from 100% of a J2-jarosite sludge, only a 25% of calcine will be available for iron recovery.

Table 2. Average chemical composition of as-received dried jarosites (wt.%) (for the sake of confidentiality, only the significant elements for the reduction process are reported).

| Sample | $Fe_2O_3$ | S | ZnO | $SiO_2$ | PbO | $Na_2O$ | CaO | $Al_2O_3$ | Other | L.O.I. |
|---|---|---|---|---|---|---|---|---|---|---|
| J1 (ED-XRF) | 33.3 | 8.9 | 7.3 | 6.4 | 5.6 | 2.8 | 1.5 | 0.7 | 3.7 | 29.8 |
| J2 (WD-XRF) | 23.9 | 29.0 | 1.2 | 5.4 | 6.1 | 1.9 | 7.6 | 0.7 | 1.2 | 23.1 |

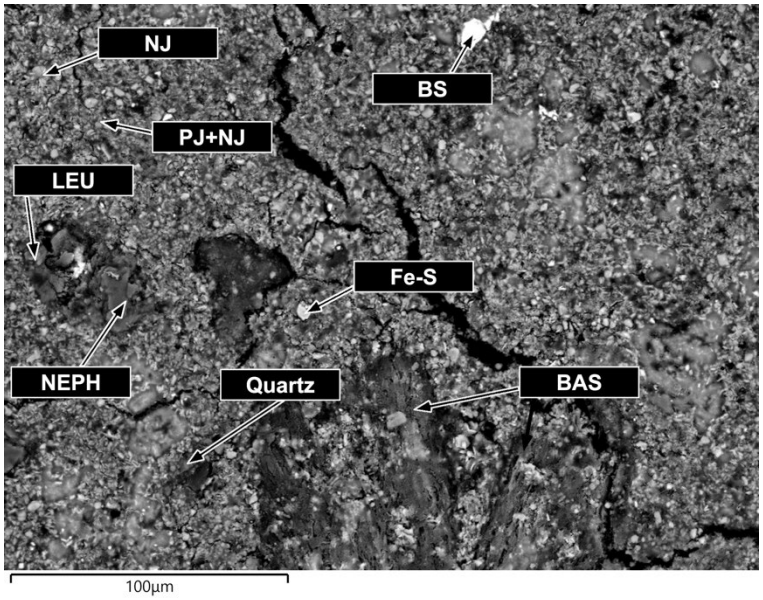


Figure 1. SEM-EDS image of as-received J2-jarosite.

Table 3. SEM-EDS analysis of as-received J2-jarosite in (at.%) (- mark means "not detected").

| Phase | Na | Al | Si | S | K | Ca | Fe | Zn | Ba | Pb |
|---|---|---|---|---|---|---|---|---|---|---|
| BAS | 0.91 | 0.59 | - | 48.38 | - | 47.56 | 2.56 | - | - | - |
| Fe-S | - | 0.31 | - | 64.36 | - | 0.09 | 34.95 | - | - | - |
| NJ | 17.39 | - | - | 36.34 | - | - | 46.27 | - | - | - |
| PJ+NJ | 9.82 | 2.74 | 8.39 | 32.18 | - | - | 43.54 | - | - | 3.33 |
| LEU | 0.27 | 18.18 | 61.02 | - | 19.34 | - | 1.19 | - | - | - |
| NEPH | 11.07 | 21.88 | 62.25 | - | 3.54 | 0.43 | 0.83 | - | - | - |
| BS | - | 1.46 | - | 46.49 | - | - | 2.48 | - | 45.31 | 0.81 |
| Quartz | - | - | 96.39 | 1.16 | - | 0.40 | 2.06 | - | - | - |
| BAS=bassanite, BS=barium sulfate, Fe-S=iron sulfide, LEU=leucite, NEPH=nepheline, NJ=natrojarosite, PJ=plumbojarosite, QZ=quartz, | | | | | | | | | | |

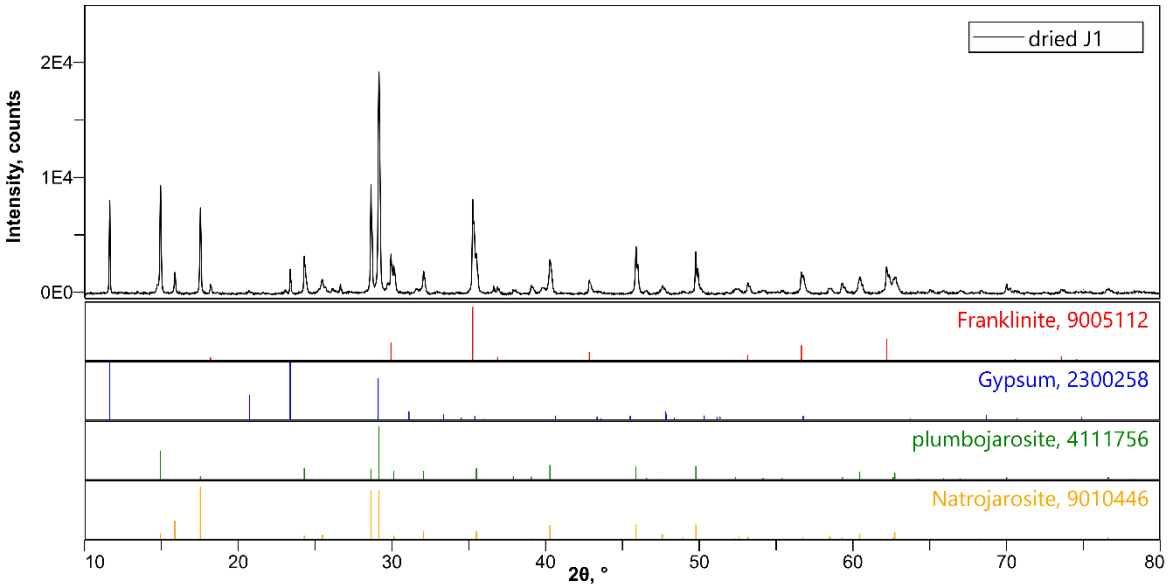


(a)

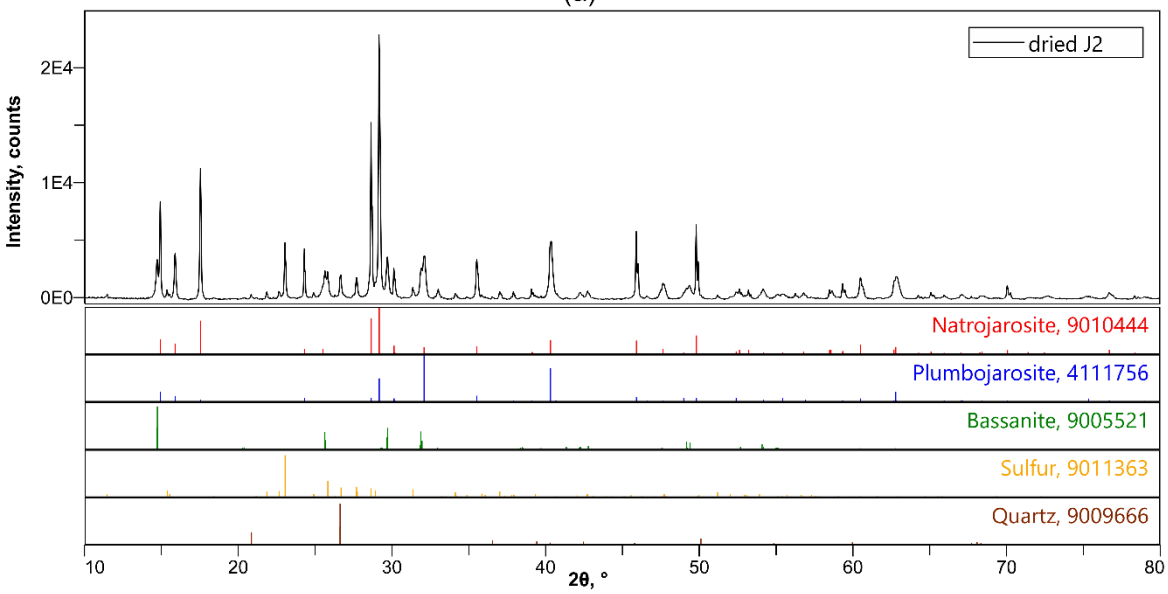


(b)

Figure 2. XRD pattern comparison between dried J1- [34] (a) and J2- (b) jarosite.

The reactions involved during J2-jarosite roasting were determined by thermogravimetry and differential scanning calorimetry on a dried jarosite sample heated up to 1000 °C (for the sake of confidentiality, the thermogram was omitted).
The TG-DSC analysis pointed out a first endothermic peak at 144 °C related to the residual moisture removal, that could involve for example the bassanite ($CaSO_4 \cdot 1/2H_2O$) dihydroxylation (Reaction 2) [46]. On the other hand, the exothermic peak at 290 °C could be related to the sulfur oxidation (Reactions 3 and 4), which is favored at low temperature [47]. It is worthy to mention that Reactions 3 and 4 were not detected in the J1-jarosite [34] and thus, they confirms the presence of elemental sulfur within the J2-jarosite.

$$CaSO_4 \cdot 1/2H_2O \rightarrow CaSO_4 \quad (2)$$

$$S + O_2 \rightarrow SO_2 \quad (3)$$

$$2SO_2 + O_2 \rightarrow 2SO_3 \quad (4)$$

Finally, the last two endothermic peaks at about 450 °C and 700 °C are related to the jarosite decomposition. More specifically, the first peak is associated to the jarosite dihydroxylation (Reactions 5 and 6), whereas, the second one is attributed to the iron sulfate decomposition into iron oxide and $SO_3$ (Reaction 7) [48,49]. Reactions 5 and 6 show an example of the possible reactions involving the natro- and plumbo-jarosite decomposition, respectively [21].

$$2NaFe_3(SO_4)_2(OH)_6 \rightarrow Na_2SO_4 + Fe_2(SO_4)_3 + Fe_2O_3 + H_2O_{(gas)} \quad (5)$$

$$PbFe_6(SO_4)_4(OH)_{12} \rightarrow PbSO_4 + Fe_2(SO_4)_3 + 2Fe_2O_3 + 6H_2O_{(gas)} \quad (6)$$

$$Fe_2(SO_4)_3 \rightarrow Fe_2O_3 + 3SO_{3(gas)} \quad (7)$$

The chemical compositions of the three conditioned materials (J1- and J2- roasted jarosite and dried BFS) are shown in Table 4. Both roasted jarosites are the main iron oxide carrier material, having more than 50 wt.% of $Fe_2O_3$. The introduction of BFS further increases the mixture final amount of available iron oxides, whereas the carbon fraction (48.9 wt.%) acts as reductant.

Table 4. Average chemical composition of roasted jarosites and dried BFS (wt.%) (- mark means "not detected") (for the sake of confidentiality, only the significant elements for the reduction process are reported).

| Sample | $Fe_2O_3$ | S | ZnO | $SiO_2$ | PbO | $Na_2O$ | CaO | $Al_2O_3$ | Other | L.O.I. | C[1] |
|---|---|---|---|---|---|---|---|---|---|---|---|
| J1 (ED-XRF) | 55.1 | 2.6 | 12.4 | 11.8 | 5.3 | 3.0 | 1.3 | 0.6 | 4.3 | 3.7 | - |
| J2 (WD-XRF) | 56.3 | 8.3 | - | 11.0 | - | 4.5 | 13.6 | 1.7 | 4.3 | 0.4 | - |
| BFS (ED-XRF) | 28.5 | 0.6 | 2.0 | 7.6 | 0.3 | 1.1 | 3.4 | 2.5 | 2.1 | 2.9 | 48.9 |
| [1]determined by elemental analysis LECO CS analyzer | | | | | | | | | | | |

Focusing on the chemical difference between the two jarosites, both are characterized by similar weight percentage of iron, silicon, and sodium oxide; contrary, the fraction of calcium oxide and sulfur in the J2-jarosite are tenfold and threefold higher than the J1-jarosite, respectively. As a consequence, in the J2-jarosite the addition of quartz instead of lime is suggested to adjust the binary basicity and obtain a value identical to the one of the J1-jarosite (0.504) used in the previous work taken as reference [36]. Furthermore, a correct binary basicity is required for the vitrification of the slag, which allow to the further safe disposal of the slag itself, as in that state it can be considered as inert [34,36].

From a mineralogical point of view, several differences are present in the two jarosite after the roasting process. As highlighted by the XRD spectra in Figure 3, in the J2-jarosite iron oxide is present exclusively as magnetite, while in the J1-sample there is the coexistence of both magnetite (and/or franklinite) and hematite. This is probably due to the different neutralization step during jarosite precipitation that leads franklinite to be discharge together with jarosite [45]. Therefore, roasted J1-jarosite shows a higher residual ZnO concentration than J2 one. Furthermore, some clustered sulfur bearing phases as galena (PbS), troilite (FeS) and sphalerite ((Zn,Fe)S) have been observed only in the J2-jarosite. These compounds are probably derived from an uncomplete oxidation during roasting of the sulphates formed after the jarosites decomposition and can be described as an intermediate situation between Reaction 6 and 7. Wollastonite ($CaSiO_3$) and nepheline ($(Na,K)AlSiO_4$) were found only in J2-jarosite, as a consequence of the high availability of CaO and $SiO_2$ featuring this sample. It is worthy to mention that wollastonite and nepheline formed during the roasting, since they were not present in the dried jarosite. Specifically, wollastonite formed by the solid-state reaction between quartz and lime freed by bassanite decomposition, while nepheline is the results of reaction between quartz, alumina and sodium freed by natrojarosite decomposition. The XRD spectra of J1-jarosite and BFS have been discussed in a previous work by Mombelli et al. and are reported here for the sake of comparison [44].

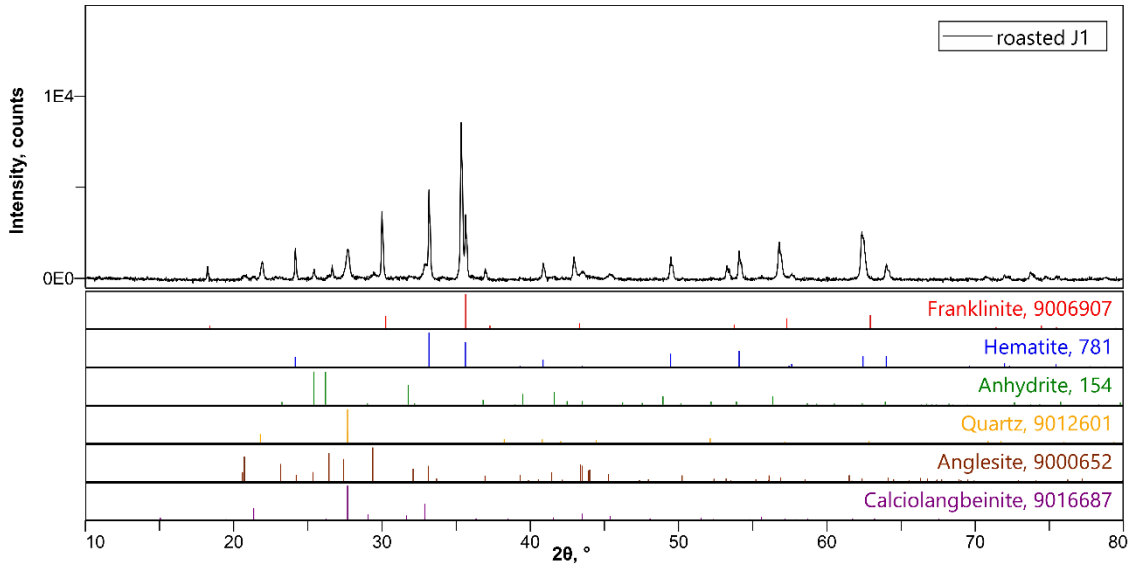


(a)

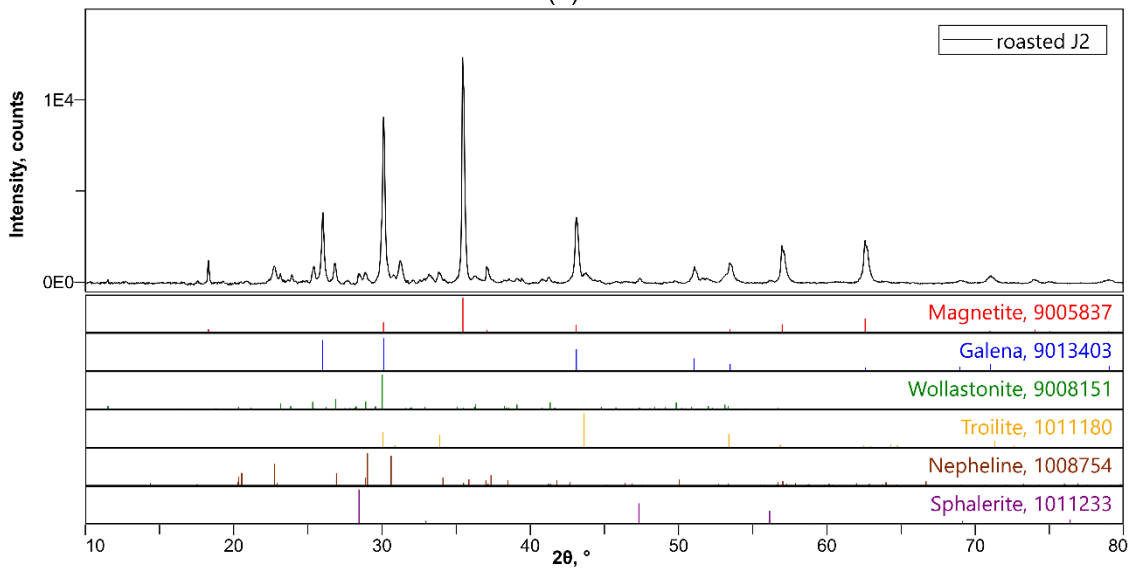


(b)

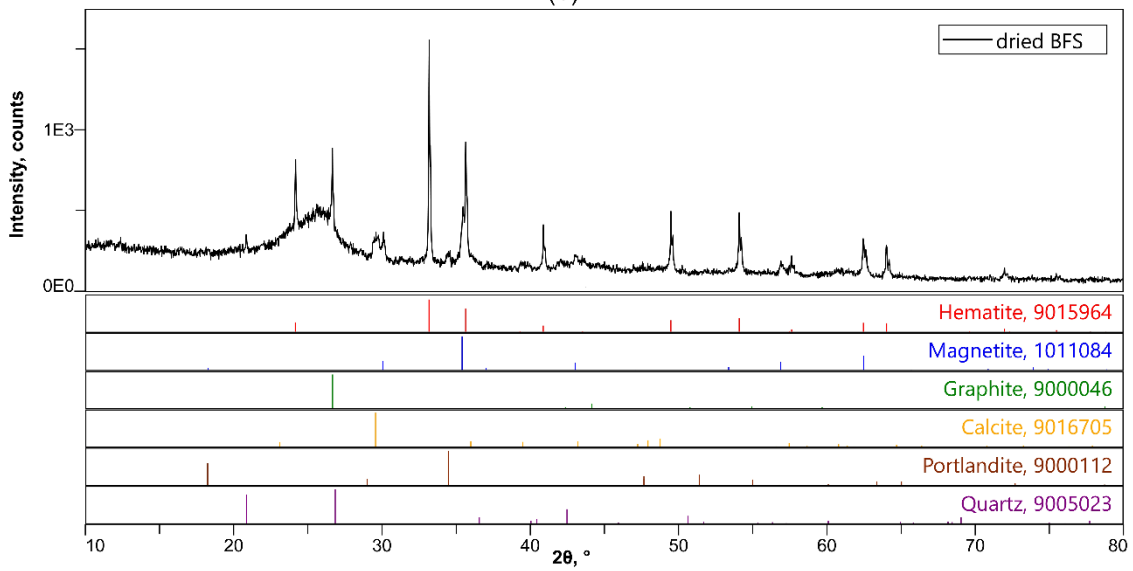


(c)

Figure 3. Conditioned materials XRD patterns: roasted J1- [34] (a) and J2- (b) jarosite; dried BFS [44] (c).

The SEM-EDS analysis carried out on the roasted J2-jarosite (Figure 4) confirmed the phases identified by XRD analysis (Table 5). In addition, leucite ($KAlSi_2O_6$) was highlighted inside the nepheline phase. However, as it was present in small amount and as most of its diffraction peaks overlaps with the ones of nepheline, its detection in the XRD spectrum could be hindered. Residual sulfides (galena, troilite and sphalerite) tend to cluster in complex phases, even if galena is the prevalent sulfide form within the roasted jarosite.

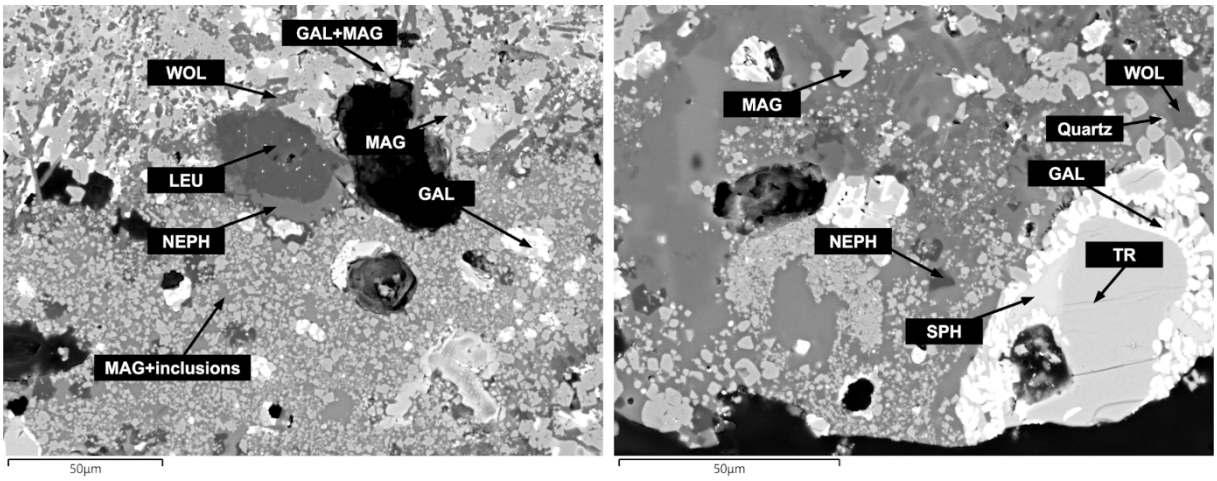


(a) (b)

Figure 4. SEM-EDS images of two roasted J2-jarosite granules (GAL=galena, LEU=leucite, MAG=magnetite, NEPH=nepheline, SPH=sphalerite, TR=troilite, WOL=wollastonite).

Table 5. SEM-EDS analysis of roasted J2-jarosite granules (at.%) (- mark means "not detected")

| Phase | Granule | Na | Al | Si | S | K | Ca | Fe | Zn | Ba | Pb |
|---|---|---|---|---|---|---|---|---|---|---|---|
| **LEU** | (a) | 2.7 | 18.41 | 60.48 | - | 17.26 | - | 1.15 | - | | - |
| **GAL** | (a) | 1.47 | 0.85 | 1.26 | 40.66 | - | 0.53 | 43.92 | - | 0.33 | 10.72 |
| **MAG** | (a) | 5.38 | 8.8 | 17.56 | 1.03 | 0.4 | 7.4 | 56.56 | 0.74 | 1.3 | 0.84 |
| **WOL** | (a) | 0.76 | 1.89 | 36.31 | 6.16 | 0.22 | 35.56 | 17.62 | - | 0.68 | 0.79 |
| **GAL+ MAG** | (a) | 1.05 | 0.64 | 24.36 | 16.33 | - | 31.83 | 11.3 | 2.34 | - | 12.15 |
| **MAG*** | (a) | 14.87 | 5.46 | 24.20 | - | 0.77 | 3.93 | 47.27 | 1.01 | 2.29 | - |
| **SPH** | (b) | 7.44 | 0.56 | - | 43.61 | - | - | 21.13 | 27.02 | - | - |
| **TR** | (b) | - | 0.41 | - | 49.59 | - | - | 49.75 | - | - | - |
| **GAL** | (b) | - | - | - | 47.82 | - | - | 33.89 | 0.31 | 0.17 | 17.5 |
| **MAG** | (b) | - | 2.08 | 1.45 | - | - | 1.35 | 93.33 | 1.11 | - | - |
| **NEPH** | (b) | 23.13 | 20.2 | 34.12 | 6.23 | 0.56 | 2.89 | 12.13 | 0.19 | 0.55 | - |
| **WOL** | (b) | - | | 47.09 | - | - | 48.88 | 3.45 | - | - | 0.59 |
| **QZ** | (b) | - | 96.39 | 1.16 | - | 0.40 | 2.06 | - | - | - | - |

GAL=galena, LEU=leucite, MAG=magnetite, MAG*= magnetite with inclusions, NEPH=nepheline, QZ=quartz, SPH=sphalerite, TR=troilite, WOL=wollastonite,

The mineralogical and chemical composition of the J2-jarosite can be exploited for specific applications in the iron metallurgy. Firstly, being iron oxide present only as magnetite the iron concentration can be increased by magnetic separation routes [50]. In addition, the low quantities of lead and zinc oxides suggests the use of briquettes made by the J2-BFS mixture as additional charging materials in the blast or cupola furnace. On the other hand, the sulfur content

could increase the amount of slag produced during the iron oxide reduction and lead to a higher coke demand [51]. Contrary, the presence of zinc in J1-jarosite represents a significant issue for the use of J1-BFS briquettes in blast furnaces. Indeed, the evaporation of zinc due to the process temperature and the subsequent condensation on the walls, at low temperature, would damage the furnace and its refractory linings [41,42]. Another aspect to be considered is the concentration of alkalis ($Na_2O$ and $K_2O$) that can hinder a profitable reuse of roasted jarosite (either J2 or J1) within the blast furnace route [52]. Consequently, cupola [53] or TSL [54] furnaces can be identified as preferable smelting plants to be fed by loose or briquetted jarosite.

### 3.2 Reducibility investigation of the J2-jarosite mixtures

The TG-DSC curves of the three J2-BFS and J1-BFS mixtures (these latter were obtained in the previous work of Mombelli et al. [36] and used as reference) are shown in Figure 5. The mixtures have the same binary basicity index (BI=0.504) and an increasing C/$Fe_2O_3$ ratio (A=0.131, B=0.261, C=0.523).

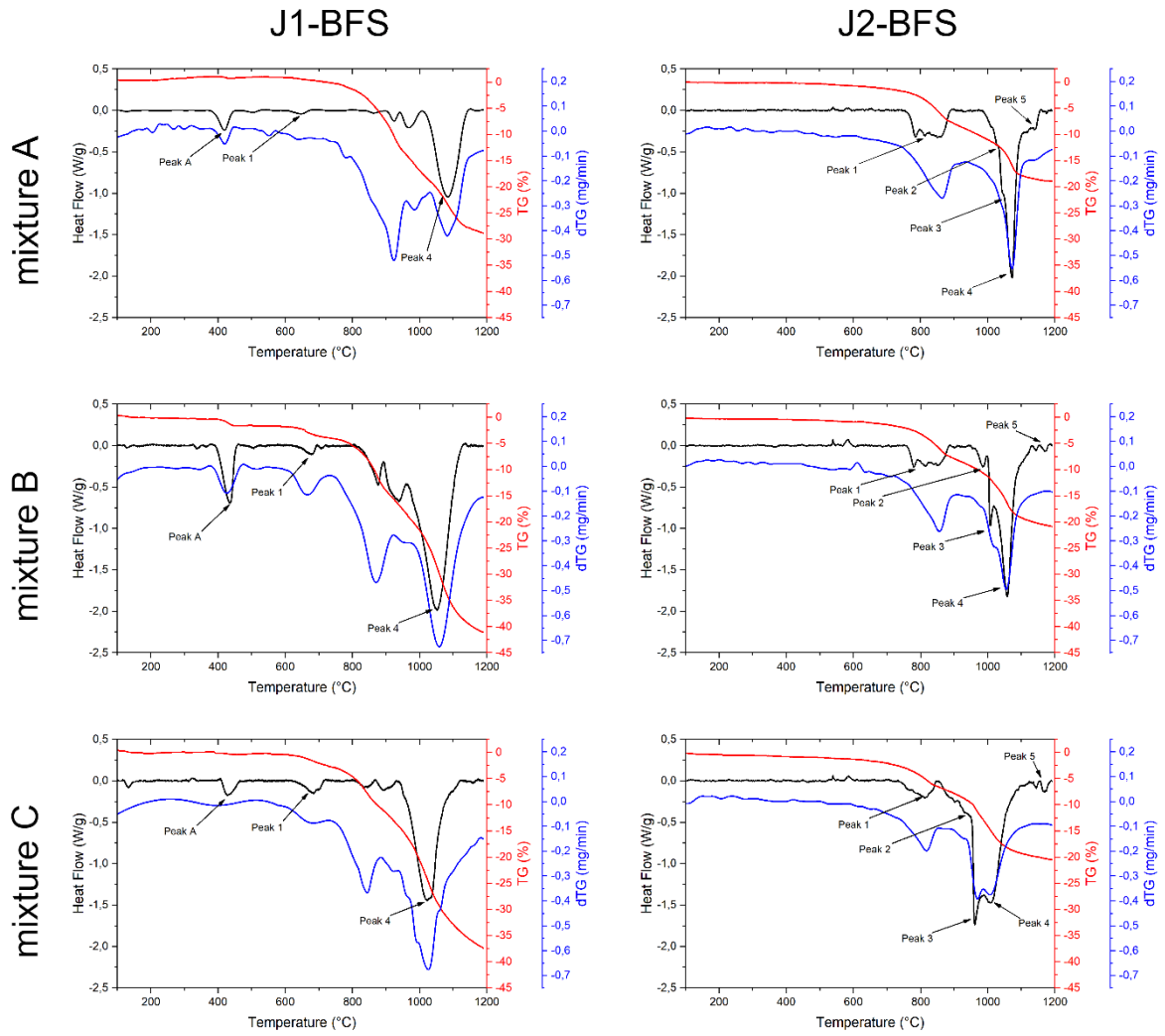


Figure 5. DSC and TG curve of the J1-BFS mixtures and J2-BFS mixtures [36].

For all six samples, two endothermic peaks are present at 750÷900 °C (Peak1) and at 1000÷1100 °C (Peak4). The first one corresponds to the calcium carbonate decomposition present in the BFS (Reaction 8), whereas the latter, more intense, refers to the iron oxide reduction and subsequent melting (Reaction 9) [55,56]. In particular, the use of an inert atmosphere during the tests inhibits the oxidation of the carbon present in the BFS, whose

concentration is high enough to reduce the FeO to Fe and significantly lower the iron melting temperature [38,56].

$$CaCO_3 \rightarrow CaO + CO_2 \qquad \Delta G = 0.0864T_{(K)} + 153.34 \qquad (8)$$

$$FeO + C \rightarrow Fe + CO \qquad \Delta G = -0.1776T_{(K)} + 171.46 \qquad (9)$$

The absence of the lime dihydroxylation peak at about 450 °C (PeakA) in the J2-BFS mixtures is due to the addition of quartz instead of lime [38]. In contrast to the three J1-BFS mixtures, whose heat flow curves are similar to each other, several differences can be observed in the J2-BFS mixtures. More precisely, in all the mixtures the Peak4 (iron reduction and melting) is preceded by two peaks (Peak2 and Peak3) while after the iron reduction a low intensity peak (Peak5) is present. Mixture C has a different heat flow profile than mixture A and B: the reduction peak has a "W" conformation due to a stronger endothermic Peak3 than mixture A and B. In all the J2-BFS mixtures Peak1 could be referred not only to the calcium carbonate decomposition but also to the lead sulfide decomposition, which seems to be confirmed by the single peak present in the dTG curves at 800 °C (Figure 6). Although it has been reported by Nafees et al. [57] that from 600 to 900 °C the evaporation of sulfur and production of metallic Pb can take place in an inert atmosphere (Reaction 10), the Gibbs free energy is positive in the all thermal range of investigation, highlighting its thermodynamical non spontaneity. On the other hand, due to the intimate contact between PbS and other oxides, a low-extent galena oxidation may also take place, leading to the formation of lead oxide, as described by Reaction 11, with (O) to be intended as bounded oxygen from other oxidic species [58]:

$$PbS \rightarrow Pb + S \qquad \begin{matrix} \Delta G = -0.0182T_{(K)} + 103.07 \ @ \ T \leq 800 \text{ K} \\ \Delta G = -0.1474T_{(K)} + 378.34 \ @ \ T \geq 900 \text{ K} \end{matrix} \qquad (10)$$

$$PbS + 3(O) \rightarrow PbO + SO_2 \qquad \Delta G = -0.278T_{(K)} + 392.14 \qquad (11)$$

Although Reaction 11 is strongly exothermic, no related peak is observed in the heat flow, probably due to the energy needed to break the chemical bond between oxygen and a generic MO-species. Thus, if this reaction happens, it is only limited to a very low extent.
Nevertheless, in the same thermal range also the reaction between PbS and PbO (present in small concentration in BFS - 0.32 wt.% - or produced by Reaction 11) may take place, with the production of sulfur oxide and lead (Reaction 12) [58], which is then removed from the mixture by evaporation at about 1000-1200 °C, since the inert atmosphere decreases the lead liquid-gas phase equilibrium temperature [59].

$$PbS + 2PbO \rightarrow 3Pb + SO_2 \qquad \Delta G = -0.2023T_{(K)} + 232.33 \qquad (12)$$

$$Fe_3O_4 + C \longrightarrow FeO + CO \qquad \Delta G = -0.2325T_{(K)} + 192.11 \qquad (13)$$

Furthermore, in affinity with the TG-DSC and dTG curves of J1-BFS, in thermal range of Peak1 also the reduction of $Fe_3O_4$ to FeO occurs (Reaction 13), which it is the responsible of the huge mass loss registered until 900 °C.
Peak2 is probably associated to albite formation and melting. Albite forms by a solid state reaction between nepheline and quartz [60]. The albite melting temperature is lower than that pointed out by the ternary system $Na_2O$-$Al_2O_3$-$SiO_2$ due to the presence of other species inside the slag (i.e., kalium and iron oxides) that act as fluxes or because the existence of an eutectic between nepheline and albite [61]. This peak is then correlated with Peak5, that probably refers to the interaction between albite and alumina crucible, since a reaction product exists on the

connection line between $Al_2O_3$ vertex and albite on the $Na_2O$-$Al_2O_3$-$SiO_2$ ternary diagram [62,63].
Finally, Peak3 could be related to the reaction of iron sulfide with hematite. As reported by Mayoral et al., oxidization of troilite by hematite is possible in the range 1000-1100 °C. However, when the contact between sulfide and oxide is intimate, the reaction temperature decreases [64]. Since the peak occurs at about 950 °C, and there is an intimate contact between iron sulfide and iron oxides, as seen in the SEM images in Figure 5, the Reaction 14 is probable. However, the above-mentioned reaction is not thermodynamically feasible, as its ΔG is positive in all the explored thermal range. In addition, as reported by Hu et al. [65], between 900 and 1000 °C the oxidation of pyrrhotite ($FeS_x$) can happen, leading to the formation of hematite. Because of troilite is a pyrrhotite with x = 1 and the condition of the mixture impose low $SO_2$ activity and intimate contact between iron sulfide and metal oxides, Reaction 15 may also locally take places. As discussed for Reaction 11, the latter is strongly exothermic but no exothermicity was revealed by heat flow. Thus, it is possible to assume that if this reaction happens, it is only to a limited extent.

$$FeS + 3Fe_2O_3 \rightarrow Fe + SO + 2Fe_3O_4 \qquad \Delta G = -0.2079T_{(K)} + 342.87 \qquad (14)$$

$$2FeS + 7(O) \rightarrow 2SO_2 + Fe_2O_3 \qquad \Delta G = -0.5483T_{(K)} + 1176 \qquad (15)$$

Furthermore, a sulfidation of hematite cannot be excluded. As reported by Han et al. [47], in the thermal range 120-1200 °C several reactions between $Fe_2O_3$, $SO_2$ and C can take place. Carbon not only promotes these sulfidation reactions but also can increase sulfur utilization rate and eliminate the generation of $SO_2$, indicating its positive role in the sulfidation of metal oxides. Additionally, the sulfidation of hematite seems to be more spontaneous at high temperature over 850 °C, in the form expressed by Reaction 16.

$$Fe_2O_3 + 2SO_2 + 7C \rightarrow 2FeS + 7CO \qquad \Delta G = -1.0415T_{(K)} + 489.81 \qquad (16)$$

Probably, among the two reactions (15,16) the last is the most probable and could also explain why in the mixture C the Peak3 is more intense than in mixture A and B and also of an intensity comparable to Peak4. Mixture C is the mix with the highest fraction of available C and probably this could enhance Reaction 16 at the expense of iron formation.
Finally, at the same temperature, an eutectic between FeS and FeO exists, which is strongly influenced by $SiO_2$ and $Na_2O$ [66]. In particular, at fixed concentration of $Na_2O$, an increase in $SiO_2$ shifts the eutectic toward smaller FeS/(FeS+FeO) ratio. Therefore, it is possible to assume that part of the unreacted FeS could melt thanks to the free silica available in the mix (~11 wt.% before heat treatment) contributing to the endothermicity of Peak3. Table 6 summarizes the most probable transformation pointed out by TG-DSC analysis and thermodynamic calculation on the J2-BFS mixtures.

Table 6. Summary of the most probable reactions during the TG-DSC analysis in J2-BFS mixtures (+: mild intensity; ++: medium intensity; +++: strong intensity).

| Peak | T [°C] | Description | Reaction | A | B | C |
|---|---|---|---|---|---|---|
| 1 | 750-900 | Calcite decomposition | $CaCO_3 \rightarrow CaO + CO_2$ | + | + | + |
| | | Galena roasting | $PbS + 2PbO \rightarrow 2Pb + SO_2$ | + | + | + |
| | | Magnetite reduction | $Fe_3O_4 + C \rightarrow 3FeO + CO$ | ++ | ++ | ++ |
| 2 | 950-1000 | Albite formation and melting | $NaAlSiO_4 + SiO_2 \rightarrow NaAlSi_3O_8$ | ++ | ++ | + |
| 3 | 975-1025 | Hematite sulfidation | $Fe_2O_3 + 2SO_2 + 7C \rightarrow 2FeS + 7CO$ | + | ++ | +++ |
| 4 | 1000-1100 | Iron oxide reduction and iron melting | $FeO + C \rightarrow Fe + CO$ | + | +++ | ++ |
| 5 | 1100-1200 | Albite-crucible reaction | $NaAlSi_3O_8 + Al_2O_3$ | ++ | + | + |

### 3.3 Characterization of the residue material in the TG-DSC crucible

The residues of the J2-BFS mixtures remained in the crucible after the TG-DSC analysis have been observed by SEM to investigate the nature of the peaks. The observation of the mixture A crucible highlighted the presence of a thin layer of slag (~30 μm) in the proximity of the crucible wall bearing undissolved alumina from to the crucible itself (Figure 6a). This occurred while the slag was still liquid, its adherence to the crucible walls implies the interaction between the alumina and the charged material, causing the following corrosion of the refractory. More in detail, the areas containing partially corroded alumina are those where the interaction did not occur completely and confirm that along the crucible walls albite (and to a lesser extent wollastonite) has reacted with alumina forming a reaction product as foreseen by the ternary diagram analysis and observed in the TG-DSC (Peak5) [63]. This assumption is further confirmed by EDS analysis (Table 7): the regions identified as albite (alb(1)) and wollastonite (wol(2)) show a concentration of Al higher than the same compounds far from the crucible walls (alb(4) and wol(5)). In addition, the traces of K and Fe, detected in the albite as impurities, lower its melting temperature, respect to the stoichiometric composition, supporting the starting hypothesis on the nature of Peak2 (Figure 5). On the contrary, the remaining two crucibles (mixture B and C) were not damaged so extensively, with their walls only locally interested by the corrosion phenomenon. This was reflected in less endothermic and visible Peak5 in the heat flow curves (Figure 5). The reduced intensity of Peak5 in mixture B and C implies that there was a limited alumina dissolution into the albite (and wollastonite). This behavior can be affected by the amount of free quartz in the mixtures, which acts both as a fluxing agent, developing binary and ternary silicate compounds, and on the overall viscosity of the slag. From mixture A to C the availability of free quartz is reduced and consequently the slag viscosity. This may have led to a reduced wettability of the crucible walls, and to a limited interaction between the slag and the crucible itself. Similarly, increasing the carbon fraction attenuates the slag melting, as observed experimentally in previous studies [56,67,68]. However, this was

never observed in any of the J1-BFS mixtures, which is probably due to the addition of lime that generally acts as viscosity reductant.

In the bottom regions of the mixture A crucible, metallic iron and iron sulfide were surrounded by wollastonite and albite (Figure 6b, Table 7). It is worthy to mention that wollastonite and albite are fully immiscible at solid state and this is reflected in the morphology of the slag phase [69].

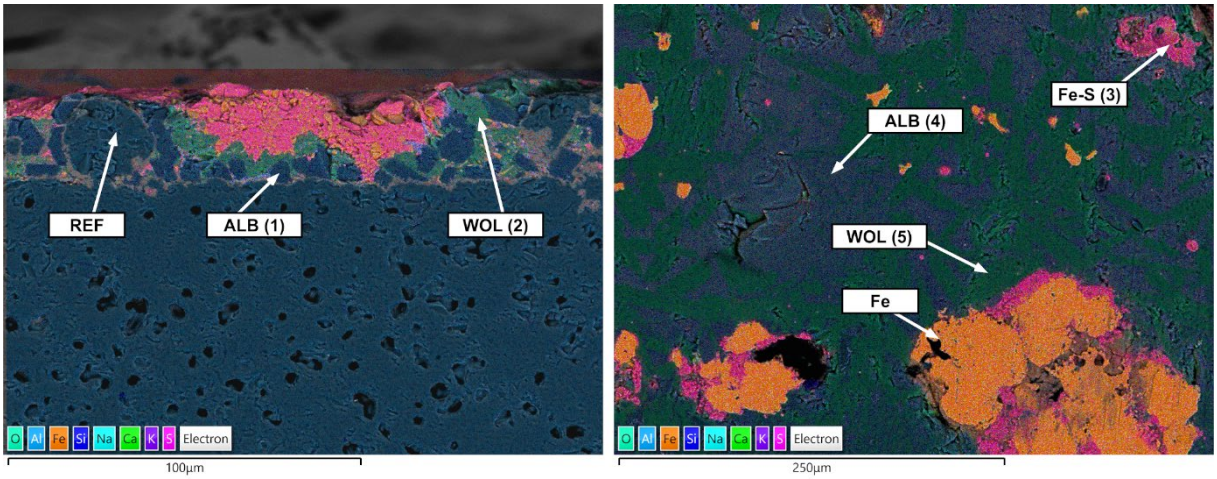


(a) (b)

Figure 6. SEM-EDS map of J2-BFS mixture A crucible wall region (a) and bottom region (b) (ALB=albite, Fe-S=iron sulfide, WOL=wollastonite).

Table 7. Slag chemical composition (at.%). Spectra referred to Figure 7 (mixture A) (- mark means "not detected").

| Spectrum | Region | Phase | Na | Al | Si | S | K | Ca | Fe |
|---|---|---|---|---|---|---|---|---|---|
| **REF** | Wall | Crucible | - | 95.94 | 3.00 | - | - | 0.17 | 0.88 |
| **1** | Wall | Albite | 15.44 | 33.08 | 41.05 | - | 4.14 | 5.02 | 1.27 |
| **2** | Wall | Wollastonite | 5.55 | 14.02 | 36.30 | - | 0.24 | 28.17 | 15.71 |
| **3** | Bottom | Iron sulfide | - | 1.50 | 1.69 | 44.52 | 0.09 | 1.70 | 50.50 |
| **4** | Bottom | Albite | 13.54 | 11.32 | 44.13 | - | 2.12 | 8.46 | 20.42 |
| **5** | Bottom | Wollastonite | 0.47 | 0.88 | 48.86 | - | - | 47.37 | 2.42 |
| **Fe** | Bottom | Metallic iron | - | 1.95 | 0.54 | - | - | - | 97.51 |

Consequently, the increased fraction of BFS in mixture B and C enhances the iron oxide reduction and decreases the slag viscosity. This can explain the increased intensity of the iron reduction and melting peak (Peak4). In addition, an excess of carbon can inhibit the coalescence of molten iron droplets and aggregation of the slag [67,68]. These consequences can explain the less compactness of slag phase and the porous morphology observed in mixture B and C (Figure 7). Despite everything, in mixture B and C the mineralogical composition remains the same as mixture A, with albite and wollastonite as the main slag phase and FeS and molten iron as the main iron-bearing compounds (Table 8). However, higher fraction of the iron sulfide is observed in these samples, which is related to the sulfidation of still not reduced hematite at the core particles at about 950 °C and thus attributable to Peak3 [57]. For all the J2-BFS mixtures, galena (present in the starting jarosite) was not observed by the SEM-EDS analysis after the

thermogravimetric tests. This confirms the complete vaporization of lead according to the reactions identified by thermal analysis.

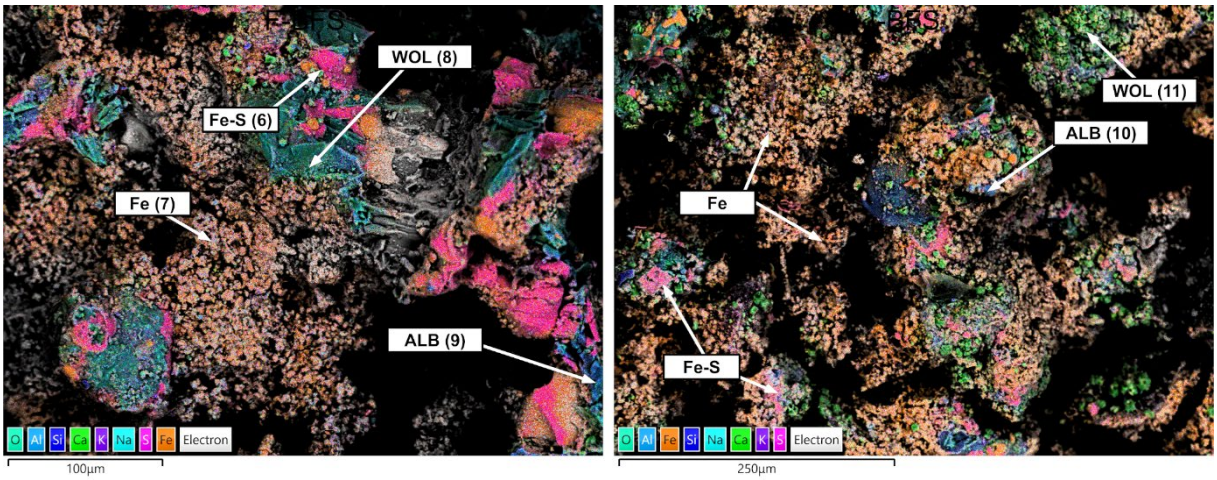


Figure 7. SEM-EDS map of J2-BFS mixture B crucible (a) and mixture C crucible (b).

Table 8. Slag chemical composition of mixtures B and C (at.%). Spectra referred to Figure 8 (- mark means "not detected").

| Spectrum | Mixture | Phase | Na | Al | Si | S | K | Ca | Fe |
|---|---|---|---|---|---|---|---|---|---|
| **6** | B | Iron sulfide | - | 1.01 | 0.55 | 47.22 | - | 0.72 | 50.51 |
| **7** | B | Fe | - | 0.97 | 0.48 | - | - | 1.24 | 97.31 |
| **8** | B | Wollastonite | 2.47 | 2.10 | 39.90 | - | - | 45.61 | 9.92 |
| **9** | B | Albite | 13.75 | 10.52 | 44.55 | 3.91 | 4.38 | 13.97 | 8.92 |
| **10** | C | Albite | 18.79 | 18.97 | 49.43 | 0.91 | 5.68 | 2.26 | 3.96 |
| **11** | C | Wollastonite | 7.72 | 8.11 | 57.71 | 1.99 | 4.79 | 15.68 | 3.98 |

### 3.4 Comparison with the theoretical model

To understand which of the three J2-BFS mixtures has the best iron oxide reduction potential, the total mass loss, peak temperature, and specific energy were evaluated by the deconvolution and integration of Peak4 by means of Origin® 2018 software and the results are shown in Figure 8. Although the possibility of using BFS as a substitute for anthracite, coke or fossil carbon for iron oxide reduction had already been investigated by Mombelli et al. [36], the J2-BFS mixtures confirmed the general trend of the reduction reaction, with the highest yield observed at a $C/Fe_2O_3$ ratio of 0.261 (mixture B). In other words, the total mass loss and the specific energy were characterized by the presence of a maximum at such $C/Fe_2O_3$ ratio. As expected, the Peak4 temperature is inversely related to the $C/Fe_2O_3$ ratio, with a decrease of about 60 °C from sample A to C ($C/Fe_2O_3$ ratio of 0.131 and 0.523, respectively). In addition, when compared with the corresponding J1-BFS mixtures (Figure 8a), the reduction reaction of the J2-BFS (Figure 8b) mixtures starts at slightly lower values (tens of degree). The lower peak temperature may be attributed to the chemical composition of the J2-jarosite. Indeed, J2-BFS mixture contains magnetite as the largest iron oxide while J1-BFS contains hematite and franklinite (approximately at a 50/50 ratio). This implies that the effective ratio of carbon to iron oxide

would be slightly higher in J2-BFS mixtures than in J1-BFS mixtures, resulting in a lower melting temperature of reduced iron and corresponding peak area [70].
Similarly, it is possible to describe the greater mass loss and specific energy observed in J1-BFS mixtures by considering the chemical composition of the starting J1-jarosite, and specifically taking into account the presence of zinc, lead and hematite within it. In fact, zinc and lead oxides are reduced and evaporate in the temperature range of Peak4 in an inert/reducing atmosphere [71].
Considering the higher oxidation state of the iron in J1-BFS mixtures, compared to the J2-BFS ones ($Fe_2O_3$ vs $Fe_3O_4$), a higher mass loss is expected, which is experimentally confirmed. In addition, since the magnetite, present in the J2-BFS mixture, is more compact than the J1-BFS mixtures hematite, the overall reaction kinetics is lowered, leading to lower iron oxide reducibility and mass loss [72].
Finally, since both the zinc and lead reduction and evaporation reactions may occur in the Peak4 temperature range, which also refers to the reduction and melting of iron, they contribute to the overall enthalpy of the peak, explaining the higher specific energy of the J1-BFS mixtures respect to the J2-BFS ones.

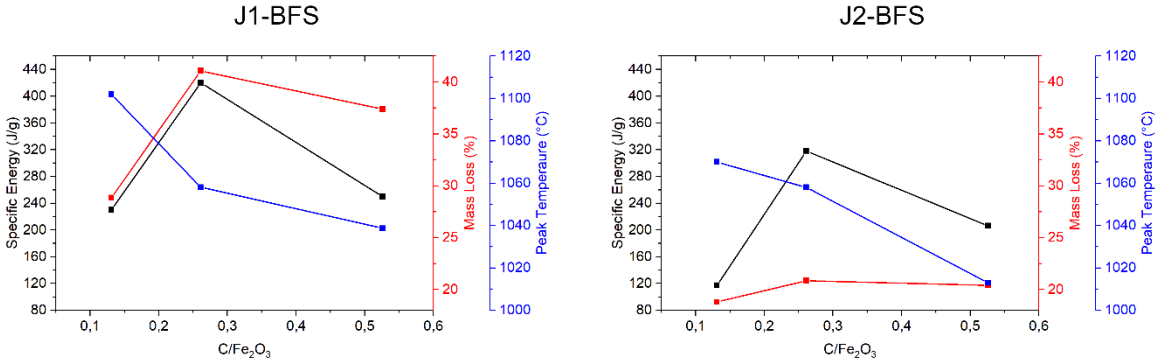


Figure 8. Specific energy, mass loss and Peak4 temperature of the J1-BFS mixtures (a) and J2-BFS mixtures (b) [36].

The theoretical mass loss ($ML_{th}$) and amount of metal produced respect to the starting charge mass ($MtC$) of the J2-BFS mixtures were compared with the experimental values ($ML_{exp}$) of the respective mixtures. The comparison allowed to validate the prediction ability of the model previously used by Mombelli et al. to study the reduction behavior of J1-BFS mixtures [36] and most importantly, understand the effect of the different chemical composition on the reduction yield of the process. The theoretical and experimental mass losses and the metal to charge ratio of the J2-BFS and J1-BFS mixtures are summarized in Table 9 and graphically showed in Figure 9.

Table 9. Theoretical and experimental values (wt.%) of the J1-BFS and J2-BFS mixtures ($ML_{th}$: foreseen mass loss by model, $ML_{exp}$: experimental mass loss, MtC: metal produced over the charge mass foreseen by the model).

| Mixture | Metal | Slag | C residue | $ML_{th}$ | $ML_{exp}$ | $\left\|\frac{ML_{th}-ML_{exp}}{ML_{exp}}\right\|$(%) | MtC |
|---|---|---|---|---|---|---|---|
| J1-BFS A | 5.65 | 94.35 | 0.00 | 31.21 | 28.83 | 8.26 | 3.89 |
| J1-BFS B | 41.12 | 58.88 | 0.00 | 43.30 | 41.08 | 5.40 | 33.38 |
| J1-BFS C | 29.42 | 55.55 | 15.03 | 38.41 | 37.38 | 2.76 | 34.21 |
| J2-BFS A | 24.50 | 75.50 | 0.00 | 18.95 | 18.87 | 0.42 | 19.85 |
| J2-BFS B | 49.88 | 49.29 | 0.83 | 23.23 | 20.75 | 11.95 | 38.29 |
| J2-BFS C | 44.24 | 41.61 | 14.15 | 22.19 | 20.50 | 8.24 | 34.42 |

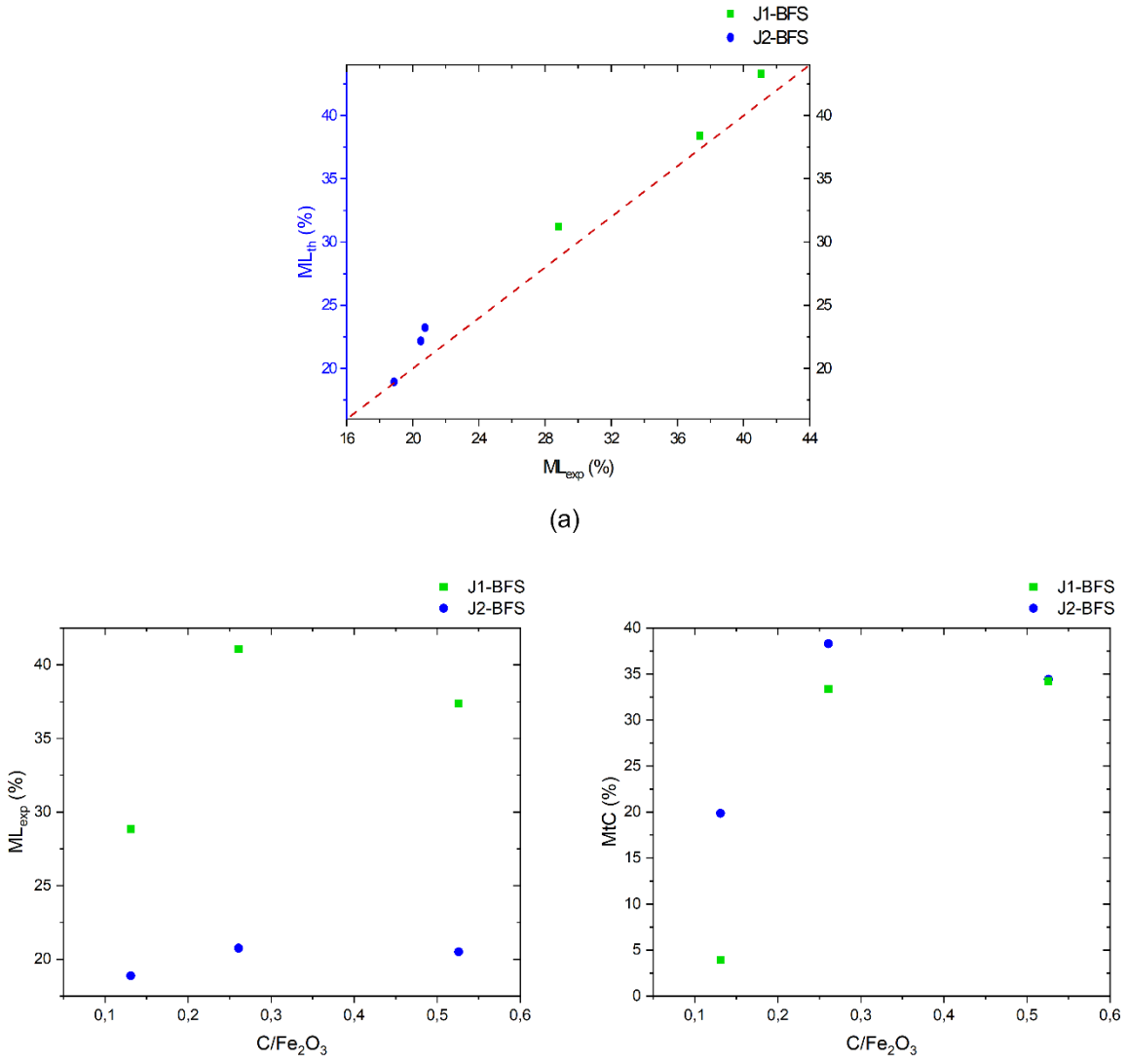


Figure 9. Comparison between the foreseen metallic loss and experimental (a), experimental mass loss (b) and theoretical metal to charge ratio (b) of the J1-BFS and J2-BFS mixtures against the carbon over iron oxide ratio.

The comparison between the experimental mass loss and the theoretical one is shown in Figure 9a: all predicted losses are slightly over the control line at 45° by about two percentage points. This divergence may be related to the initial assumptions that the order of the reduction reactions follows exactly the Ellingham diagram, with a complete conversion of the oxides, without considering the kinetics or dynamic evolution of the gases partial pressure. In fact, the complete vaporization of $Na_2O$ and $K_2O$ was assumed in the model, however their presence was evidenced as albite in the J2-BFS mixtures slag by SEM analysis.
Furthermore, the presence of alkali oxides can inhibit the self-reduction capability of the mixtures due to the generation of localized liquid phases rich in iron oxide, which fills the pores, reducing gas diffusion, and consequently the reaction kinetics [73].
The inverse relationship between the amount of slag and the $C/Fe_2O_3$ ratio, previously observed by Mombelli et al. [36], and experimentally observed by SEM-EDS analysis, is also confirmed by the theoretical model values (Figure 9b-c). The amount of mass loss which can be related to the effective charge reduction has the same trend for both J2-BFS and J1-BFS mixtures with a maximum of reducibility at a $C/Fe_2O_3$ of 0.261 (mixture B). However, J1-BFS mixtures are characterized by a twofold mass loss compared to the J2-BFS ones. On the other hand, *MtC*, which can be related to the metal production, shows a slightly different behavior: J2-BFS has a maximum metal production at 0.261 $C/Fe_2O_3$, while J1-BFS has practically the same productivity at 0.261 and 0.523. These differences in behavior seem strongly influenced by the presence of zinc (and to a lesser extent lead) in the J1 one. According to the Ellingham diagram, the reduction and evaporation of zinc oxide should occur before that of wustite, which corresponds to the last stage before iron production. Consequently, most of the mass loss observed in J1-BFS mixtures can be attributed to the removal of the volatile fraction from the mixture. On the other hand, J2-BFS mixtures do not experience significant changes in mass loss as the $C/Fe_2O_3$ ratio increases. The assumption that most of the mass loss in the J1-BFS is associated with zinc oxide reduction is confirmed by the theoretical *MtC* ratio, whose values are comparable to those experimentally obtained by Mombelli et al. in a previous work and by the absence of zinc-containing compounds in the slag [36].
In comparison, the J2-BFS mixtures yield is far higher than that of J1-BFS ones when a low amount of carbon is available (mixture A). On the other hand, as the $C/Fe_2O_3$ ratio increases, the difference between the two mixtures *MtC* decreases and becomes convergent at the mixture C composition. Probably this is due to a dilution effect operated by the BFS on the volatile compounds within the J1-jarosite.

### 3.5 Metallurgical process applicability

The possibility of exploiting the reducing property of the jarosite-BFS mixtures in the metallurgical processes to recover iron is highly appealing. However, the direct introduction of these mixtures in the form of powders would lead to several environmental and human health problems during their use and transportation due to the high proportion of fines [74].
The agglomeration of powders in the form of briquettes or pellets overcomes these problems, while also increasing the overall management (handling, storage, charging and chemical composition) of the agglomerated product. In addition, several metallurgical processes are already experimenting with the addition of agglomerate-product in the starting feedstock to recover and valorize different types of waste materials [75–80].
As for the present work, the introduction of jarosite-BFS mixtures into the metallurgical process would be constrained by the starting chemistry of the agglomerated product, assuming the development of the required mechanical properties.
The low percentage of Zn and Pb in the J2-BFS allows their introduction in the blast furnace, after proper agglomeration, even though particular attention should be paid to the amount of Na and K, that could also generate some issues during the process [81,82]. Similarly, the high initial concentration of S could inhibit the use of jarosite as iron-ore substitute. Nowadays, since

modern ironmaking blast furnaces operate at lower temperature to keep Si in the iron under the 1 wt.%, more S contaminates the molten bath. This is not a problem, since S can be efficiently removed both at the pretreatment station before conversion or after steelmaking in dedicate secondary metallurgy facilities (i.e., ladle furnace) [83].

Contrary, the introduction in the blast furnace of agglomerate products made from J1-BFS mixtures is strongly discouraged due to the presence of undesirable and harmful elements for the process itself (e.g., S, K, Zn, Na and Pb) [84]. Furthermore, the high percentage of zinc in the J1-jarosite, which is responsible of the lower reduction yield compared to the J2-BFS mixtures, would further hinder the applicability of the J1-BFS agglomerates products.

Consequently, the application of specific pretreatments, (both pyrometallurgical and hydrometallurgical) to J1-BFS mixtures would be highly suggested prior to their introduction into the blast furnace and for the recovery of specific and valuable elements such as Zn [70,85–87]. Zhang et al., investigated the sulfidation and sulfur fixation at different carbon additions of a Chinese jarosite with a chemical composition close to that of J1-sample [70]. However, such pretreatment would not be suitable for subsequent introduction into the blast furnace, as these elements would not be removed from the mixture, but only transformed into stable phases. In contrast, selective chlorination could remove most of the Zn and Pb present in the J1-jarosite, allowing its introduction into the blast furnace [85,87].

In contrast, cupola furnaces are able to charge the agglomerates produced by both mixtures, as the process allows the introduction of higher percentages of Zn, Pb, Na and K. Furthermore, most of the Zn and Pb would be removed inside the cupola furnace itself due to the high temperature achieved, whereas most of the iron would be reduced over a short period of time (20-30 min) [36,44,53,88].

Finally, the Metso Outotec's Ausmelt® TSL furnace appears as the most suitable candidate for both the mixtures charging, even without any kind of pretreatment or agglomeration, as the process itself was design to accommodate and recover valuable metals from low-grade concentrates with high amount of iron, zinc, lead and others [89,90].

## 4 Conclusions

Following the promising results obtained from the use of blast furnace sludge for the reduction of an industrial jarosite previously characterized, this work investigates the effect of the different chemical composition of another industrial jarosite sample, that differs from the previous in S, Pb, Ca and Zn concentration, on the self-reduction capacity of the jarosite plus blast furnace sludge mixture. The main differences and similarities of the two jarosite and respective mixtures behavior can be summarized as follows:

- The amount of calcium oxide in the J2-jarosite is ten times higher respect to the J1 one. As a consequence, the J2-jarosite is characterized by a binary basicity of about 1, which suggests the addition of quartz as fluxing agent instead of lime to keep constant the desired basicity of the mixture (0.504).
- J2-BFS mixtures are characterized by higher reduction yield respect to the J1-BFS ones for each of the three mixtures. Among them, the J2-BFS mixture B (BFS/jarosite=0.36, $C/Fe_2O_3$=0.261) leads to the best iron oxide reduction, which is coherent with the results obtained using the J1-jarosite.
- The values of mass loss and slag amount predicted by the application of the theoretical model, previously used on the J1-BFS mixtures, to the J2-BFS mixtures slightly overestimated the experimental values (with an error of less than 10%) and confirmed the overall reduction behavior of the mixtures.

The characterization results allow to infer that:

- The low amount of lead and zinc oxides in the starting J2-jarosite would allow its introduction in both the blast and cupola furnace processes after their agglomeration with BFS or in the Metso Outotec's Ausmelt® TSL furnace without agglomeration.
- Contrary, J1-BFS mixtures should be subject to zinc recovery pretreatments to increase the iron reduction yield and match the chemical composition limitations for the blast furnace charging. On the other hand, they could be introduced without any pretreatments in the cupola furnace after agglomeration or in the Metso Outotec's Ausmelt® TSL furnace without agglomeration.

In conclusion, the reducibility of the jarosite plus blast furnace sludges seems not affected by the starting jarosite chemical composition from the general process point of view, although only two samples of jarosite seem too little to represent all the jarosite as well. However, very close to 0.261 $C/Fe_2O_3$ ratio given the best reduction on other two different jarosites, supporting the above conclusion [70,85]. On the other hand, the chemical composition of the J2-jarosite expands its possibilities for introduction into metallurgical processes as additional charging material. At the same time, pretreatment of J1-jarosite could be a solution to achieve the same scope and reduction yield and specially to recover the Zn it contains. Finally, with the growing interest in the industrial byproducts recycling, the agglomeration of the J2-BFS and J1-BFS mixtures appears as an innovative alternative for the recovery of iron and other valuable metals contained in the jarosite with a consequent reduction of the environmental impact of the metallurgical industry.

**Acknowledgements**

The Authors would like to acknowledge Dr. Marco Alloni (Prosimet S.p.A. – Filago (BG), Italy) for TG-DSC and XRF analysis on as-supplied and roasted jarosite. Acknowledgements also go to Dr. Mario Ragona and Centro Ricerche Ecotec for supplying the raw jarosites.

**Funding**

This research was supported by the Italian Ministry for Education, University and Research (MIUR) through the "Department of Excellence LIS4.0" project (Integrated Laboratory for Lightweight and Smart Structures).

**Conflict of interest declaration**

On behalf of all authors, the corresponding author states that there is no conflict of interest.

**Authors statement**

**Davide Mombelli:** conceptualization, methodology, visualization, writing - original draft. **Gianluca Dall'Osto**: writing – original draft, review and editing, resources. **Valentina Trombetta**: formal analysis, investigation, data curation, writing – original draft. **Carlo Mapelli**: supervision.

**References**

[1] A.J. Monhemius, The iron elephant: A brief history of hydrometallurgists' struggles with element no. 26, CIM J. 8 (2017). https://doi.org/10.15834/cimj.2017.21.

[2] R.M. Grant, Zinc Production, Encycl. Mater. Sci. Technol. (2001) 9891–9894. https://doi.org/10.1016/b0-08-043152-6/01790-3.

[3] S. Seyer, T.T. Chen, J.E. Dutrizac, Jarofix: Addressing iron disposal in the zinc industry, Jom. 53 (2001) 32–35. https://doi.org/10.1007/s11837-001-0010-2.

[4] J.E. Dutrizac, J.L. Jambor, Jarosites and Their Application in Hydrometallurgy, Rev. Mineral. Geochemistry. 40 (2000) 405–452. https://doi.org/10.2138/rmg.2000.40.8.

[5] M. Cruells, A. Roca, Jarosites: Formation, Structure, Reactivity and Environmental, Metals (Basel). 12 (2022) 802. https://doi.org/10.3390/met12050802.
[6] J.E. Dutrizac, S. Kaiman, Synthesis and properties of jarosite-type compounds, Can. Mineral. 14 (1976) 151–158.
[7] J.E. Dutrizac, Factors affecting alkali jarosite precipitation, Metall. Trans. B. 14 (1983) 531–539.
[8] J.M. Bigham, F.S. Jones, B. Özkaya, E. Sahinkaya, J.A. Puhakka, O.H. Tuovinen, Characterization of jarosites produced by chemical synthesis over a temperature gradient from 2 to 40 C, Int. J. Miner. Process. 94 (2010) 121–128.
[9] J.E. Dutrizac, J.L. Jambor, The behaviour of arsenic during jarosite precipitation: arsenic precipitation at 97 C from sulphate or chloride media, Can. Metall. Q. 26 (1987) 91–101.
[10] J.E. Dutrizac, T.T. Chen, The Behaviour of Gallium During Jarosite Precipitation, Can. Metall. Q. 39 (2000) 1–14. https://doi.org/10.1179/cmq.2000.39.1.1.
[11] J.E. Dutrizac, D.J. Hardy, T.T. Chen, The behaviour of cadmium during jarosite precipitation, Hydrometallurgy. 41 (1996) 269–285. https://doi.org/10.1016/0304-386X(95)00062-L.
[12] J.E. Dutrizac, T.T. Chen, The behaviour of scandium, yttrium and uranium during jarosite precipitation, Hydrometallurgy. 98 (2009) 128–135. https://doi.org/10.1016/j.hydromet.2009.04.009.
[13] J.E. Dutrizac, T.T. Chen, The behaviour of phosphate during jarosite precipitation, Hydrometallurgy. 102 (2010) 55–65.
[14] O.H. Tuovinen, L. Carlson, Jarosite in cultures of iron-oxidizing thiobacilli, Geomicrobiol. J. 1 (1979) 205–210.
[15] F.S. Jones, J.M. Bigham, J.P. Gramp, O.H. Tuovinen, Synthesis and properties of ternary (K, NH4, H3O)-jarosites precipitated from Acidithiobacillus ferrooxidans cultures in simulated bioleaching solutions, Mater. Sci. Eng. C. 44 (2014) 391–399.
[16] S.I. Grishin, J.M. Bigham, O.H. Tuovinen, Characterization of jarosite formed upon bacterial oxidation of ferrous sulfate in a packed-bed reactor, Appl. Environ. Microbiol. 54 (1988) 3101–3106.
[17] G.K. Das, S. Acharya, S. Anand, R.P. Das, Jarosites: A review, Miner. Process. Extr. Metall. Rev. 16 (1996) 185–210. https://doi.org/10.1080/08827509708914135.
[18] A. Pappu, M. Saxena, S.R. Asolekar, Jarosite characteristics and its utilisation potentials, Sci. Total Environ. 359 (2006) 232–243. https://doi.org/10.1016/j.scitotenv.2005.04.024.
[19] J.E. Dutrizac, J.L. Jambor, Behaviour of cesium and lithium during the precipitation of jarosite-type compounds, Hydrometallurgy. 17 (1987) 251–265.
[20] J.E. Dutrizac, S. Kaiman, Rubidium jarosite and thallium jarosite—new synthetic jarosite-type compounds and their structures, Hydrometallurgy. 1 (1975) 51–59.
[21] F.L. Forray, A.M.L. Smith, C. Drouet, A. Navrotsky, K. Wright, K.A. Hudson-Edwards, W.E. Dubbin, Synthesis, characterization and thermochemistry of a Pb-jarosite, Geochim. Cosmochim. Acta. 74 (2010) 215–224. https://doi.org/10.1016/j.gca.2009.09.033.
[22] T. Chen, L. Cabri, Mineralogical overview of iron control in hydrometallurgical processing., in: 1996.
[23] T.T. Chen, J.E. Dutrizac, A Mineralogical Study of Jarofix Products for the Stabilization of Jarosite Residues for Disposal, in: Lead-Zinc 2000, John Wiley & Sons, Inc., Hoboken, NJ, USA, 2013: pp. 917–934. https://doi.org/10.1002/9781118805558.ch63.
[24] J.E. Dutrizac, The Behavior of Impurities during Jarosite Precipitation, in: Hydrometall. Process Fundam., Springer US, Boston, MA, 1984: pp. 125–169. https://doi.org/10.1007/978-1-4899-2274-8_6.
[25] M. Kerolli-Mustafa, L. Ćurković, H. Fajković, S. Rončević, Ecological risk assessment

681 of jarosite waste disposal, Croat. Chem. Acta. 88 (2015) 189–196.
682 https://doi.org/10.5562/cca2554.
683 [26] Y. Song, M. Wang, J. Liang, L. Zhou, High-rate precipitation of iron as jarosite by using
684 a combination process of electrolytic reduction and biological oxidation,
685 Hydrometallurgy. 143 (2014) 23–27. https://doi.org/10.1016/j.hydromet.2014.01.003.
686 [27] D. Zhu, C. Yang, J. Pan, Z. Guo, S. Li, New pyrometallurgical route for separation and
687 recovery of Fe, Zn, In, Ga and S from jarosite residues, J. Clean. Prod. 205 (2018) 781–
688 788. https://doi.org/10.1016/j.jclepro.2018.09.152.
689 [28] M. Rämä, S. Nurmi, A. Jokilaakso, L. Klemettinen, P. Taskinen, J. Salminen, Thermal
690 Processing of Jarosite Leach Residue for a Safe Disposable Slag and Valuable Metals
691 Recovery, Metals (Basel). 8 (2018) 744. https://doi.org/10.3390/met8100744.
692 [29] E. Salinas, A. Roca, M. Cruells, F. Patiño, D.. Córdoba, Characterization and alkaline
693 decomposition–cyanidation kinetics of industrial ammonium jarosite in NaOH media,
694 Hydrometallurgy. 60 (2001) 237–246. https://doi.org/10.1016/S0304-386X(01)00149-9.
695 [30] I.A. Reyes, F. Patiño, M.U. Flores, T. Pandiyan, R. Cruz, E.J. Gutiérrez, M. Reyes, V.H.
696 Flores, Dissolution rates of jarosite-type compounds in H2SO4 medium: A kinetic
697 analysis and its importance on the recovery of metal values from hydrometallurgical
698 wastes, Hydrometallurgy. 167 (2017) 16–29.
699 https://doi.org/10.1016/j.hydromet.2016.10.025.
700 [31] A. Roca, J. Viñals, M. Arranz, J. Calero, Characterization and Alkaline
701 Decomposition/Cyanidation of Beudantite–Jarosite Materials From RIO Tinto Gossan
702 Ores, Can. Metall. Q. 38 (1999) 93–103. https://doi.org/10.1179/cmq.1999.38.2.93.
703 [32] F. Patiño, J. Viñals, A. Roca, C. Núñez, Alkaline decomposition-cyanidation kinetics of
704 argentian plumbojarosite, Hydrometallurgy. 34 (1994) 279–291.
705 https://doi.org/10.1016/0304-386X(94)90066-3.
706 [33] A. Roca, F. Patiño, J. Viñals, C. Núñez, Alkaline decomposition-cyanidation kinetics of
707 argentojarosite, Hydrometallurgy. 33 (1993) 341–357. https://doi.org/10.1016/0304-
708 386X(93)90071-K.
709 [34] D. Mombelli, C. Mapelli, C. Di Cecca, S. Barella, A. Gruttadauria, M. Ragona, M. Pisu,
710 A. Viola, Characterization of cast iron and slag produced by jarosite sludges reduction
711 via Arc Transferred Plasma (ATP) reactor, J. Environ. Chem. Eng. 6 (2018) 773–783.
712 https://doi.org/10.1016/j.jece.2018.01.006.
713 [35] L. Ye, Z. Peng, L. Wang, A. Anzulevich, I. Bychkov, D. Kalganov, H. Tang, M. Rao, G.
714 Li, T. Jiang, Use of Biochar for Sustainable Ferrous Metallurgy, Jom. 71 (2019) 3931–
715 3940. https://doi.org/10.1007/s11837-019-03766-4.
716 [36] D. Mombelli, C. Mapelli, S. Barella, A. Gruttadauria, E. Spada, Jarosite wastes reduction
717 through blast furnace sludges for cast iron production, J. Environ. Chem. Eng. (2019).
718 https://doi.org/10.1016/j.jece.2019.102966.
719 [37] S.S. Rath, D.S. Rao, S.K. Tripathy, S.K. Biswal, Characterization vis-á-vis utilization of
720 blast furnace flue dust in the roast reduction of banded iron ore, Process Saf. Environ.
721 Prot. 117 (2018) 232–244. https://doi.org/10.1016/j.psep.2018.05.007.
722 [38] D. Mombelli, C. Di Cecca, C. Mapelli, S. Barella, E. Bondi, Experimental analysis on
723 the use of BF-sludge for the reduction of BOF-powders to direct reduced iron (DRI)
724 production, Process Saf. Environ. Prot. 102 (2016) 410–420.
725 https://doi.org/10.1016/j.psep.2016.04.017.
726 [39] D. Mombelli, S. Barella, A. Gruttadauria, C. Mapelli, Iron recovery from Bauxite
727 Tailings Red Mud by thermal reduction with blast furnace sludge, Appl. Sci. 9 (2019).
728 https://doi.org/10.3390/app9224902.
729 [40] BAT, Best Available Techniques – Reference document for iron and steel production:
730 Industrial emissions directive 2010/75/EU: integrated pollution prevention and control,
731 Reference Report by the Joint Research Centre of the European Commission, 2012.

732 [41] H. Ahmed, New Trends in the Application of Carbon-Bearing Materials in Blast Furnace
733 Iron-Making, Minerals. 8 (2018) 561. https://doi.org/10.3390/min8120561.
734 [42] S.S. Ashrit, R. V. Chatti, S. Sarkar, Identification of the carbon source in blast furnace
735 flue dust through characterisation and statistical analysis, Int. J. Environ. Anal. Chem.
736 101 (2021) 1378–1392. https://doi.org/10.1080/03067319.2019.1682142.
737 [43] N.P. Nayak, Characterization of blast furnace flue dust- an assessment for its utilization,
738 Mater. Today Proc. 50 (2022) 2078–2083. https://doi.org/10.1016/j.matpr.2021.09.417.
739 [44] D. Mombelli, D.L. Gonçalves, C. Mapelli, S. Barella, A. Gruttadauria, Processing and
740 Characterization of Self-Reducing Briquettes Made of Jarosite and Blast Furnace
741 Sludges, J. Sustain. Metall. (2021). https://doi.org/10.1007/s40831-021-00419-2.
742 [45] 911 Metallurgist, Jarosite production, (n.d.). https://www.911metallurgist.com/jarosite-
743 production/ (accessed May 26, 2022).
744 [46] W.E.P. Fleck, M.H. Jones, R.A. Kuntze, H.G. McAdie, The differential thermal analysis
745 of natural and synthetic hydrates of calcium sulphate, Can. J. Chem. 38 (1960) 936–943.
746 https://doi.org/10.1139/v60-131.
747 [47] J. Han, W. Liu, T. Zhang, K. Xue, W. Li, F. Jiao, W. Qin, Mechanism study on the
748 sulfidation of ZnO with sulfur and iron oxide at high temperature, Sci. Rep. 7 (2017)
749 42536. https://doi.org/10.1038/srep42536.
750 [48] C. Drouet, K.L. Pass, D. Baron, S. Draucker, A. Navrotsky, Thermochemistry of jarosite-
751 alunite and natrojarosite-natroalunite solid solutions, Geochim. Cosmochim. Acta. 68
752 (2004) 2197–2205. https://doi.org/10.1016/j.gca.2003.12.001.
753 [49] H.H.A. J. Laurence Kulp, Thermal study of jarosite, (n.d.).
754 [50] J. Tenório Vinhal, R. Húngaro Costa, J. Luís Coleti, D.C.R. Espinosa, Iron recovery from
755 zinc mine tailings by magnetic separation followed by carbothermal reduction of self-
756 reducing briquettes, Can. J. Chem. Eng. 99 (2021) 166–177.
757 https://doi.org/10.1002/cjce.23845.
758 [51] A. Babich, D. Senk, H.W. Gudenau, K.T. Mavrommatis, Ironmaking Textbook,
759 Verlagshaus Mainz GmbH, Aachen, 2008.
760 [52] A. Bhattacharyya, J. Schenk, G. Rantitsch, C. Thaler, H. Stocker, Effect of alkaline
761 elements on the reactivity, strength and structural properties of blast furnace cokes,
762 Metalurgija. 54 (2015) 503–506.
763 [53] M. Holtzer, A. Kmita, A. Roczniak, The Recycling of Materials Containing Iron and
764 Zinc in the OxyCup Process, Arch. Foundry Eng. 15 (2015) 126–130.
765 [54] J. Wood, J. Coveney, G. Helin, L. Xu, S. Xincheng, The Outotec ® Direct Zinc Smelting
766 Process, in: Proc. Pb-Zn, 2015: pp. 1–13.
767 [55] H. Song, Y. Jeong, S. Bae, Y. Jun, S. Yoon, J. Eun Oh, A study of thermal decomposition
768 of phases in cementitious systems using HT-XRD and TG, Constr. Build. Mater. 169
769 (2018) 648–661. https://doi.org/10.1016/j.conbuildmat.2018.03.001.
770 [56] D.J.C. Stewart, A. Scrimshire, D. Thomson, P.A. Bingham, A.R. Barron, The chemical
771 suitability for recycling of zinc contaminated steelmaking by-product dusts: The case of
772 the UK steel plant, Resour. Conserv. Recycl. Adv. 14 (2022) 200073.
773 https://doi.org/10.1016/j.rcradv.2022.200073.
774 [57] M. Nafees, M. Ikram, S. Ali, Thermal stability of lead sulfide and lead oxide nano-
775 crystalline materials, Appl. Nanosci. 7 (2017) 399–406. https://doi.org/10.1007/s13204-
776 017-0578-7.
777 [58] A.M. Abdel-Rehim, Thermal and XRD analysis of Egyptian galena, J. Therm. Anal.
778 Calorim. 86 (2006) 393–401. https://doi.org/10.1007/s10973-005-6785-6.
779 [59] D. Ghosh, Removal of lead from Fe-Pb mixtures by evaporation in stagnant argon at
780 1448 K and the determination of the lead vapor-argon interdiffusivity, ISIJ Int. 50 (2010)
781 673–677. https://doi.org/10.2355/isijinternational.50.673.
782 [60] R.V. Dietrich, Feldspathoid, Encycl. Br. (n.d.).

https://www.britannica.com/science/feldspathoid (accessed May 27, 2022).
[61] G. Sen, Phase Relations in Simple Systems: Key to Magma Generation, Crystallization, and Mixing, in: Petrology, Springer Berlin Heidelberg, Berlin, Heidelberg, 2014: pp. 51–78. https://doi.org/10.1007/978-3-642-38800-2_3.
[62] Verein Deutscher Eisenhüttenleute (VDEh), ed., Slag Atlas (Schlackenatlas), 2nd ed., Verlag Stahleisen GmbH, Dusseldorf, 1995.
[63] D.A. Brosnan, Corrosion of Refractories, in: C.A. Schacht (Ed.), Refract. Handb., Marcel Dekker Inc., Pittsburgh (PA), 2004: pp. 39–79. https://doi.org/10.1201/9780203026328.
[64] M.C. Mayoral, M.T. Izquierdo, J.M. Andrés, B. Rubio, Impact of iron-sulfide deposits on oxidized austenitic steels as simulation of corrosion and fireside-tube wastage in coal combustion, Oxid. Met. 59 (2003) 395–407. https://doi.org/10.1023/A:1023052313584.
[65] G. Hu, K. Dam-Johansen, S. Wedel, J.P. Hansen, Decomposition and oxidation of pyrite, Prog. Energy Combust. Sci. 32 (2006) 295–314. https://doi.org/10.1016/j.pecs.2005.11.004.
[66] H. Shamazaki, L.A. Clark, Liquidus relations in the FeS-FeO-SiO 2-Na 2O system and geological implications, Econ. Geol. 68 (1973) 79–96. https://doi.org/10.2113/gsecongeo.68.1.79.
[67] D.J.C. Stewart, D. Thomson, A.R. Barron, The production of high value pig iron nuggets from steelmaking by-products – A thermodynamic evaluation, Resour. Conserv. Recycl. 170 (2021) 105592. https://doi.org/10.1016/j.resconrec.2021.105592.
[68] H. Han, D. Duan, S. Chen, P. Yuan, Mechanism and Influencing Factors of Iron Nuggets Forming in Rotary Hearth Furnace Process at Lower Temperature, Metall. Mater. Trans. B. 46 (2015) 2208–2217. https://doi.org/10.1007/s11663-015-0420-0.
[69] W.R. Foster, The System <tex-math>$NaAlSi_{3}O_{8}-CaSiO_{3}-NaAlSiO_{4}$</tex-math>, J. Geol. 50 (1942) 152–173. http://www.jstor.org/stable/30068449.
[70] B. Zhang, L. Zhu, W. Liu, J. Han, F. Jiao, W. Qin, Sulfidation and Sulfur Fixation of Jarosite Residues During Reduction Roasting, Metall. Mater. Trans. B Process Metall. Mater. Process. Sci. 50 (2019) 761–771. https://doi.org/10.1007/s11663-019-01517-z.
[71] R. Busè, D. Mombelli, C. Mapelli, Metals recovery from furnaces dust: Waelz process, La Metall. Ital. 106 (2014) 19–27.
[72] W. Nicodemi, C. Mapelli, Siderurgia, 1st Editio, Milano, 2011.
[73] W. Pan, Z.J. Ma, Z.X. Zhao, W.H. Kim, D.J. Min, Effect of Na2O on the reduction of Fe2O3 compacts with CO/CO2, Metall. Mater. Trans. B Process Metall. Mater. Process. Sci. 43 (2012) 1326–1337. https://doi.org/10.1007/s11663-012-9738-z.
[74] R. Cappelletti, M. Ceppi, J. Claudatus, V. Gennaro, Health status of male steel workers at an electric arc furnace (EAF) in Trentino, Italy, J. Occup. Med. Toxicol. 11 (2016) 7. https://doi.org/10.1186/s12995-016-0095-8.
[75] A. Andersson, A. Gullberg, A. Kullerstedt, A. Wedholm, J. Wikström, H. Ahmed, L.S. Ökvist, Recycling of Blast Furnace Sludge to the Blast Furnace via Cold-Bonded Briquettes: Evaluation of Feasibility and Influence on Operation, ISIJ Int. 59 (2019) 1786–1795. https://doi.org/10.2355/isijinternational.ISIJINT-2019-080.
[76] N.A. El-Hussiny, M.E.H. Shalabi, A self-reduced intermediate product from iron and steel plants waste materials using a briquetting process, Powder Technol. 205 (2011) 217–223. https://doi.org/10.1016/j.powtec.2010.09.017.
[77] S. Wu, F. Chang, J. Zhang, H. Lu, M. Kou, Cold strength and high temperature behaviors of self-reducing briquette containing electric arc furnace dust and anthracite, ISIJ Int. (2017) ISIJINT--2017.
[78] V. Singh, V. Tathavadker, Development of Agglomeration Process to Utilize the Ferromanganese Fines in Steel Making Process, ISIJ Int. 51 (2011) 59–62.

https://doi.org/10.2355/isijinternational.51.59.
[79] M.C. Bagatini, T. Fernandes, R. Silva, D.F. Galvão, I. V. Flores, Mill scale and flue dust briquettes as alternative burden to low height blast furnaces, J. Clean. Prod. 276 (2020) 124332. https://doi.org/10.1016/j.jclepro.2020.124332.
[80] L.R. Lemos, S.H.F.S. da Rocha, L.F.A. de Castro, G.B.M. Assunção, G.L.R. da Silva, S.H.F.S. da Rocha, L.F.A. de Castro, G.B.M. Assunção, G.L.R. da Silva, Mechanical strength of briquettes for use in blast furnaces, REM - Int. Eng. J. 72 (2019) 63–69. https://doi.org/10.1590/0370-44672017720156.
[81] T. Hilding, S. Gupta, V. Sahajwalla, B. Björkman, J.O. Wikström, Degradation behaviour of a high CSR coke in an Experimental Blast Furnace: Effect of carbon structure and alkali reactions, ISIJ Int. 45 (2005) 1041–1050. https://doi.org/10.2355/isijinternational.45.1041.
[82] A.A. El-Geassy, K.A. Shehata, M.I. Nasr, S.S. Fakhoury, EFFECT OF ALKALIES ON THE PERFORMANCE OF BLAST FURNACE., Trans. Iron Steel Inst. Japan. 26 (1986) 865–874. https://doi.org/10.2355/isijinternational1966.26.865.
[83] S. Barella, C. Di Cecca, C. Mapelli, A. Gruttadauria, E. Bondi, A. Marinari, Study of a New Operating Practice for Refining High Silicon Hot Metal in a BOF Converter, Steel Res. Int. 87 (2016) 941–946. https://doi.org/10.1002/srin.201500283.
[84] A. Samolejová, R. Lenort, P. Besta, A. Samolejová, K. Janovská, R. Lenort, J. Haverland, The effect of harmeful elements in production of iron in relation to input and output material balance, Metalurgija. 51 (2012) 325–328. https://www.researchgate.net/publication/285013253.
[85] Y. Wang, H. Yang, G. Zhang, J. Kang, C. Wang, Comprehensive recovery and recycle of jarosite residues from zinc hydrometallurgy, Chem. Eng. J. Adv. 3 (2020) 100023. https://doi.org/10.1016/j.ceja.2020.100023.
[86] A. Maihatchi Ahamed, M.N. Pons, Q. Ricoux, S. Issa, F. Goettmann, F. Lapicque, New pathway for utilization of jarosite, an industrial waste of zinc hydrometallurgy, Miner. Eng. 170 (2021) 107030. https://doi.org/10.1016/j.mineng.2021.107030.
[87] L. Höber, K. Witt, S. Steinlechner, Selective Chlorination and Extraction of Valuable Metals from Iron Precipitation Residues, Appl. Sci. 12 (2022) 3590. https://doi.org/10.3390/app12073590.
[88] J.S.F. Carter, US2643185A - Cupola melting of cast iron, 1950.
[89] M.A. Reuter, J. Wood, S. Creedy, R. Matusewicz, M. Reuter, Secondary copper processing using Outotec Ausmelt TSL technology, in: Proc. MetPlant, 2011: pp. 460–467.
[90] J. Wood, J. Coveney, G. Helin, L. Xu, S. Xincheng, The Outotec ® Direct Zinc Smelting Process, in: Proc. EMC, 2015: pp. 1–13.